UNIVERSITY OF AMSTERDAM

UvA-DARE (Digital Academic Repository)

Chain Character of Vacancy-Type Defects in Silicon

Sieverts, E.G.; Sprenger, M.; Ammerlaan, C.A.J.

DOI
10.1103/PhysRevB.41.8630
Publication date
1990

Published in
Physical Review. B, Condensed Matter

Link to publication

Citation for published version (APA):
Sieverts, E. G., Sprenger, M., & Ammerlaan, C. A. J. (1990). Chain Character of Vacancy-Type Defects in Silicon. *Physical Review. B, Condensed Matter*, *41*, 8630-8642. https://doi.org/10.1103/PhysRevB.41.8630

General rights
It is not permitted to download or to forward/distribute the text or part of it without the consent of the author(s) and/or copyright holder(s), other than for strictly personal, individual use, unless the work is under an open content license (like Creative Commons).

Disclaimer/Complaints regulations
If you believe that digital publication of certain material infringes any of your rights or (privacy) interests, please let the Library know, stating your reasons. In case of a legitimate complaint, the Library will make the material inaccessible and/or remove it from the website. Please Ask the Library: https://uba.uva.nl/en/contact, or a letter to: Library of the University of Amsterdam, Secretariat, Singel 425, 1012 WP Amsterdam, The Netherlands. You will be contacted as soon as possible.

UvA-DARE is a service provided by the library of the University of Amsterdam (https://dare.uva.nl)

Download date:10 Mar 2023

Chain character of vacancy-type defects in silicon

E. G. Sieverts, M. Sprenger, and C. A. J. Ammerlaan
Natuurkundig Laboratorium der Universiteit van Amsterdam, Valckenierstraat 65, NL-1018 XE Amsterdam, The Netherlands
(Received 15 December 1989)

With electron-nuclear double resonance the hyperfine interactions between a paramagnetic defect electron and large numbers of silicon lattice sites have been determined for a number of vacancy-related defects, viz., two charge states of the divacancy and the negative charge states of the vacancy and the oxygen-vacancy complex. In all four cases a prominent series of interactions can be distinguished that can be identified with lattice sites on a single [011]-oriented zigzag lattice chain that emanates on both sides from the vacant lattice site(s). Additional experiments on the negative divacancy have corroborated this picture. The probability density of the electron wave function is by far most pronounced on this chain, while its decrease with distance along the chain is appreciably slower than in any other direction. In all cases about 80% of the unpaired defect electron is localized in such a chain, while within experimental uncertainty the density along the chain decreases exponentially at the same rate for all defects. A comparison with theoretical calculations of charge densities is made. The relation between this one-dimensional extended electronic structure and the so-called fifth-neighbor interaction for the diamond lattice is more firmly established.

I. INTRODUCTION

During the past several years extensive information has been gathered about hyperfine interactions with ^{29}Si nuclei around defects and impurities in silicon. Within the distinct classes of paramagnetic centers pronounced similarities were observed. For the vacancy-related defects in silicon already from electron paramagnetic resonance (EPR) measurements such similarities have become apparent. A characteristic trademark for these defects is the occurrence of a large hyperfine interaction with one or more equivalent neighbor atoms at which dangling bonds are present. In a description of the unpaired defect electron, as constituted from a linear combination of atomic orbitals (LCAO), these largest hyperfine interactions already account for a localization of about 60% of the electron.

From electron-nuclear double resonance (ENDOR) experiments on the two paramagnetic charge states of the divacancy (V-V^+ and V-V^-), it was noted that also for more remote neighbors in the mirror plane in which the two dangling bonds are situated, the localization of the unpaired electron is more pronounced than elsewhere. This followed from a simple supposition of monotonic decrease of the wave function with distance within the distinct types of neighbor sites.[1] More recently, Sprenger recognized in ENDOR data from the negative vacancy (V^-) a whole series of very similar hyperfine interactions, whose magnitudes decrease at a surprisingly constant rate.[2,3] These interactions were identified as arising from silicon atoms in a single [011]-oriented zigzag chain of the silicon lattice, which includes the vacancy and the two main dangling bonds. A suggestion for a similar structure had already been made in 1961 by Watkins and Corbett, just from some barely resolved hyperfine interactions in the EPR spectrum of the oxygen-vacancy complex (O-V^-).[4] Extensive ENDOR experiments have recently been performed on this same defect system. Apart from other similarities with the vacancy, a nearly exact replica of the [011] chain in the vacancy has been recognized in these (O-V^-) ENDOR data.[5,6]

In the present work these data are further assessed. In addition, ENDOR results of the positive and negative divacancy[7-9] are reanalyzed in a similar manner. Moreover, important additional experimental data for the negative divacancy have been obtained. All these data present strong evidence that in all four defects the unpaired electron is localized in highly similar [011] lattice chains that contain the two main dangling bonds of the defects. Thanks to the lower symmetry of the divacancy, a directional ambiguity which was still present in the detailed interpretation of the V^- and O-V^- hyperfine interactions can now be removed.

Theoretical calculations by Kane[10] have demonstrated a preferential charge localization along similar ⟨011⟩ lattice chains around a charge disturbance at a substitutional site of tetrahedral symmetry. These results will be discussed in some detail and be compared with the present experimental results. In his work, Kane showed the importance of so-called fifth-neighbor interactions for a proper description of the vibrations of covalent solids and its influence on the charge distribution.[10,11] The relation between the detailed electronic and atomic defect structure in the ⟨011⟩ lattice chains and the structural disturbances as produced by these fifth-neighbor interactions will be assessed in more detail. Other examples of such zigzag charge transfer will also be given.

Finally, the consequences for the remainder of the defect wave functions after identification of the [011]-chain hyperfine interactions are discussed and compared for the different defects.

 ©1990 The American Physical Society

II. EXPERIMENTAL DATA

A. General analysis of experimental results

All experimental data that will be discussed here have been obtained from ENDOR experiments on electron irradiated monocrystalline silicon. For a complete description of the production of the various defects and for a discussion on the ENDOR technique, we refer to previous papers.[2,3,5–9] These papers also contain comprehensive treatments of the spin Hamiltonians which describe the observed ENDOR spectra and of the symmetry arguments which allow discrimination between hyperfine interactions from lattice sites in different symmetry classes. Consequently, we will discuss these points only concisely.

All defects discussed in this paper are paramagnetic because of a single unpaired electron spin and can thus be described with $S=\frac{1}{2}$. In addition, silicon contains a natural abundance of 4.7% of the isotope ^{29}Si which has a nuclear spin $I=\frac{1}{2}$. Between electron spin and nuclear spins hyperfine interactions will be present. For a magnetic resonance experiment the defect systems can effectively be described with a spin Hamiltonian with electronic and nuclear Zeeman interaction and hyperfine interaction, in which a summation is made over the interactions with the various surrounding magnetic nuclei:

$$\mathcal{H}=\mu_B \mathbf{B}\cdot\overleftrightarrow{g}\cdot\mathbf{S}+\sum_i(-g_N\mu_N\mathbf{B}\cdot\mathbf{I}_i+\mathbf{S}\cdot\overleftrightarrow{A}_i\cdot\mathbf{I}_i)\ . \tag{1}$$

In this paper only the hyperfine interaction will be of importance as it is directly related to the wave function of the unpaired electron. The hyperfine tensor is mostly decomposed as

$$\overleftrightarrow{A}_i=a_i\overleftrightarrow{1}+\overleftrightarrow{B}_i\ . \tag{2}$$

The isotropic Fermi-contact interaction a_i is related to the probability of the electron wave function at the nuclear site:

$$a_i=\tfrac{2}{3}\mu_0 g\mu_B g_N\mu_N|\Psi(r_i)|^2\ . \tag{3}$$

The anisotropic part $\overleftrightarrow{B}_i$ describes the dipole-dipole interaction. If an LCAO description of the wave function is chosen, this tensor is, to a first approximation, only determined by the atomic p orbitals at the pertinent atom. For a single atomic p orbital a purely axial interaction should result, with its axis along the orbital direction and with principal values $(2b_i,-b_i,-b_i)$, where

$$b_i=(\mu_0/4\pi)g\mu_B g_N\mu_N\tfrac{2}{5}\langle r^{-3}\rangle_p\ . \tag{4}$$

The wave-function parameters as derived from the experimental data with Eqs. (2)–(4) can be compared with the values $|\psi_s(0)|^2=34.6\times10^{30}$ m^{-3} and $\langle r^{-3}\rangle_p=\langle\psi_p|r^{-3}|\psi_p\rangle=18.2\times10^{30}$ m^{-3} for full atomic $3s$ and $3p$ orbitals in free-silicon atoms.[12] This gives direct information about the fractions of s and p orbitals at particular atomic sites, that contribute to the LCAO wave function. In practice, the interactions in these lower-symmetry systems are never exactly axially symmetric. By decomposing the principal values of $\overleftrightarrow{B}$ as $(2b,-b+c,-b-c)$ the deviation from axial symmetry is measured by c.

All four defects discussed have lower-than-tetrahedral point-group symmetry. The presence of a magnetic ^{29}Si nucleus at a neighbor site can lower the symmetry even further. On the basis of characteristic anisotropic angle-dependent patterns, the observed hyperfine interactions can be ascribed to classes of neighbor sites of a certain symmetry. The EPR spectra of V^- and O-V^- indicate $2mm$ defect symmetry. In that case we can discriminate between hyperfine interactions with four types of lattice sites: on two different $\{011\}$ mirror planes, on a twofold axis, or at other positions. For V-V^+ and V-V^- with $2/m$ mirror plane symmetry, we can only discriminate between sites on the mirror plane or outside the plane. For a further assignment of hyperfine interactions to particular lattice sites within the classes of neighbor sites, no direct experimental evidence exists. However, on the basis of interpretation and a phenomenological analysis, several assignments could be made.

B. Vacancy and oxygen-vacancy complex

For the negative vacancy (V^-) hyperfine interactions with 51 shells of neighbor sites, containing 152 lattice sites, could be determined. From these 51 different interactions 18 were with sites in the $(0\bar{1}1)$ mirror plane of the defect, which also contains the two dangling bonds, called the *ad* plane.[2] These interactions were labeled *Mad*1–*Mad*18. With lattice sites in the other mirror plane, the (011) or *bc* plane, only five interactions, labeled *Mbc*1–*Mbc*5, were observed. This was consistent with the theoretical consideration of antisymmetry with respect to the *bc* plane, making it a "forbidden" plane for the defect wave function. From the 51 interactions 17 did not comply with an LCAO description of the defect wave function, mostly because they were not even approximately axially symmetric. Of particular interest are the 18 interactions in the *ad* mirror plane. Ten of them form a subset with remarkably similar properties. Formally these similarities can be defined by the following criteria: (i) the interactions have a very small deviation from [111] axiality (less than ~12%) and the axial direction is in the mirror plane; (ii) the principal direction perpendicular to the mirror plane belongs to the second largest principal value; (iii) both the ratios a/b and b/c have approximately the same values for the different sites. Especially when looking at the corresponding angular-dependent patterns, their visual similarity and their distinct difference from other observed interactions are striking.[13] Numerical data on these interactions are given in Table I and in Refs. 2 and 13. Although the third characteristic does not apply to the largest interaction, tensor *Mad*1 is also considered to belong to this group. It is generally assumed that *Mad*1 arises from the nearest-neighbor atoms of the vacancy. This is in accord with the predicted a-d molecular orbital for the unpaired electron.[14] It is now argued that the next hyperfine interaction of this group, *Mad*2, arises from the next-neighbor shells in the *ad*-mirror plane, connected by $\langle 111\rangle$ bonds to the nearest neighbors. In a covalent solid this is not unreasonable, as atom-atom bonds play the

TABLE I. Parameters of *Mad*-class interactions of V^- and O-V^- that belong to the chain group. Given are quotients of hyperfine parameters a/b and b/c, fractions s-character α^2 and localizations η^2 on pertinent neighbor shells, and deviations δ from nearest $[\bar{1}11]$ or $[\bar{1}\,\bar{1}\,\bar{1}]$ direction.

Interaction	a/b	b/c	α^2	η^2 (%)	δ (deg)
		V^-			
*Mad*1	15.9	17.7	0.28	27.28	−0.1
*Mad*2	9.2	8.3	0.18	5.90	−0.3
*Mad*3	8.3	12.6	0.17	3.88	1.7
*Mad*4	9.0	9.7	0.18	1.60	−0.5
*Mad*5	8.5	11.9	0.18	0.79	−1.2
*Mad*6	8.5	11.6	0.18	0.38	−1.0
*Mad*8	9.1	11.7	0.18	0.18	−2.1
*Mad*12	8.9	13.9	0.18	0.10	−1.8
*Mad*14	8.8	15.8	0.18	0.05	−3.4
*Mad*17	8.8	15.0	0.18	0.02	−3.4
		O-V^-			
*Mad*1	17.2	21.4	0.30	29.98	0.9
*Mad*2	9.6	7.6	0.20	4.44	3.1
*Mad*3	9.2	9.1	0.19	3.06	6.2
*Mad*4	12.3	9.4	0.24	1.63	3.2
*Mad*5	9.8	11.9	0.20	0.71	1.3
*Mad*6	9.9	11.6	0.20	0.38	3.1
*Mad*8	11.2	8.7	0.22	0.16	1.8
*Mad*9	11.2	13.3	0.22	0.11	1.8
*Mad*13	9.7	12.0	0.20	0.04	0.4
*Mad*18	10.8	8.8	0.21	0.03	1.2

dominant role in the constitution of the crystal lattice. This suggests an identification of the hyperfine interactions from the present group with lattice sites in a planar zigzag chain along the [011] direction. The somewhat exceptional position of *Mad*1 in the group is ascribed to the occurrence of lattice distortions so close to the vacant lattice site. In the discussion to follow, this deviation will be made even more plausible.

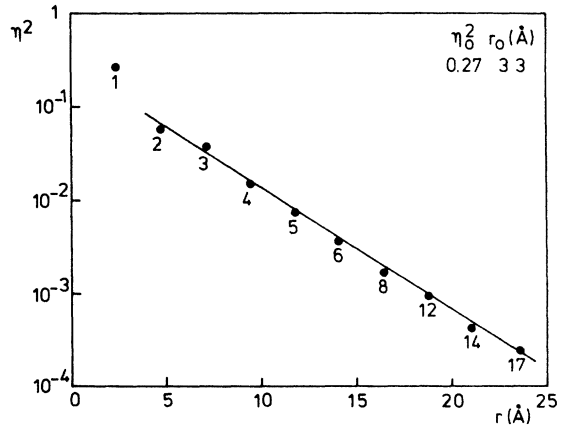

FIG. 1. Localization η^2 of the wave function of the negative vacancy as a function of the distance to the vacancy, measured along the [011] zigzag chain. Numbers refer to the chosen *Mad*-type hyperfine interactions. The line represents a logarithmic fit to the formula $\eta(r)^2=\eta_0^2\exp(-r/r_0)$. Tensor *Mad*1 is not included in the fit.

For all interactions the localization η^2 of the unpaired electron has been determined by simply adding the calculated contributions from s and p atomic orbitals as derived from Eqs. (3) and (4).[2] When assuming that the interactions of the above-defined group belong to lattice sites of just a single [011]-oriented zigzag lattice string in the *ad* plane, and that the magnitude of the interactions decreases monotonically with the distance to the vacancy, their values η^2 can be plotted against this distance. The resulting semi-logarithmic plot is shown in Fig. 1. Except for tensor *Mad*1, all points are found to fall on an

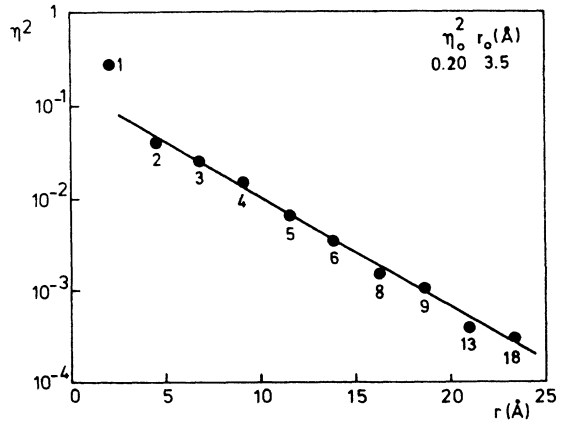

FIG. 2. Localization η^2 of the wave function of the negative oxygen-vacancy complex. Further details as in Fig. 1.

excellent straight line. The total resulting localization on this chain amounts to 80%. In the underlying model of a pseudo-one-dimensional defect, the defect wave function extends very far along this chain. The last tensor *Mad* 17 lies at a straight distance of 19.2 Å. As to its distance, this position constitutes the 53rd *Mad* shell. There exist even some 1500 lattices sites within a sphere of this radius, while only 150 have a larger hyperfine interaction.

For the negative oxygen-vacancy complex (O-V^-) very similar results have been obtained.[5,6] Fifty hyperfine interactions could be determined, twenty of which were of the *Mad* type. In keeping with the same criteria as for the vacancy, a similar group of ten *Mad* tensors fell aside. Under the same assumptions the resulting electron localizations can be plotted against the distance to the vacancy along the [011] chain. Figure 2 shows that a nearly identical plot results, indicative for identically [011] extended wave functions for both defects.

C. Divacancy

The present analysis can also be extended to the divacancy. For both charge states of this defect, a much smaller number of interactions had been determined. As a result, statistics were somewhat less convincing than for V^- and O-V^-. So far, 19 interactions had been determined for V-V^+, seven of which belonged to the mirror-plane type M.[7,8] For V-V^- 33 interactions were known, 13 of which were of the M type.[9] When carefully considering these M-type interactions, in essentially the same way, for both defects a group of similar interactions manifests itself. For V-V^+ they satisfy the first two criteria as formulated for the vacancy. For the degree of axiality as given by b/c, although sufficiently large for the whole group, some more variation must be accepted than for the vacancy. For V-V^- in one case it is not very obvious which tensor to choose. Tensors $M5$, $M8$, and $M9$ are quite similar, with the same axial direction and with η^2 values which are close together. The only distinction is that tensor $M9$ has a larger deviation of its axial direction. Since only one of the tensors can fit into a regular sequence, as a somewhat arbitrary choice, $M5$ is taken. Among the V-V^- tensors, the condition for the direction of the second principal axis is not satisfied for all tensors of the special group. This does not seem too serious, however, as especially in these cases the axiality is extremely good, so that a distinction between second and third principal value has hardly any meaning. For b/c the same applies as observed for V-V^+.

Knowing the special properties of the hyperfine interactions of this category, it is easy to extend ENDOR experiments in order to selectively reveal these interactions. This procedure, applied to V-V^-, has indeed resulted in the determination of two more tensors which fit fairly well in the same pattern. Moreover, a number of additional tensors of both symmetry classes could be determined as well. For this purpose ENDOR measurements have been performed on EPR transitions of the divacancy orientations *ad*, *da*, *bc*, and *cb*, in the way as described in Refs. 2 and 9. The magnetic field was rotated at 2.5° intervals in the $(0\bar{1}1)$ plane. For directions in this plane the orientations *bc* and *cb* are degenerate. Tensors for mirror-plane class interactions are completely determined by the angular dependence of just these four defect orientations. General class tensors cannot unambiguously be determined in this way. Additional measurements in the [100], [111], and [011] directions for the other orientations are, in principle, sufficient to solve uncertainties in this case. As a result of the strong overlap between the patterns in the region for hyperfine interactions smaller than 400 kHz, it was often hard to decide which branches of the angular dependent patterns of the general class tensors exactly belong together. Therefore, the complete determination of these new general class tensors needs not be 100% reliable, in contrast to the other ones. However, for the discussion in Sec. IV C in which these data are used, this is of minor importance. Data for the new tensors, six of the M class and seven of the G class, are given in Table II. Including the new data, the number of tensors analyzed for V-V^- is now raised to 46.

The relevant properties of the M-class hyperfine interactions of V-V^+ and V-V^-, including the new ones which have been chosen to belong to the chain, are collected in Table III. Resulting plots for both defects are shown in Fig. 3. The similarity of the plots for all four different defects can be made more quantitative by comparing the straight lines which result from a least-squares fit in the semilogarithmic plots. In all cases the first point, from the interaction with the nearest neighbors, has been left out, because it diverges too far. The lines are described by $\eta(r)^2=\eta_0^2\exp(-r/r_0)$. The resulting parameters η_0^2 and r_0 are given in Table IV.

III. THEORETICAL DATA

The simplest description of a defect wave function has been given for a one-dimensional model semiconductor. Lannoo and Lenglart[15] used it as an introduction to their calculation on the vacancy in diamond, as it allowed an analytical solution. They adopted a tight-binding approximation, using the Green's-function formalism. For their one-dimensional semiconductor they determined the band structure of a perfect linear chain, taking *sp* hybridized atomic orbitals. Introduction of a vacancy resulted in a bound state for which the contributions from the atomic orbitals could be determined. Orbitals pointing outward to the next atom, as seen from the vacancy, were found not to contribute. Contributions from orbitals pointing inward were found to decrease with a constant factor for each next atom. This means that there is an exponential decrease with distance, just as in our experimental observations. The decrease rate is determined by the free-atom energies of the *s* and *p* orbitals, and by the interaction between neighboring orbitals in this linear structure. Estimates for these values result in a factor of the order of only 1.2 between adjacent sites, while in the [011] chain in the real three-dimensional crystal we found, experimentally, a factor of about 2.

Recently Kane[10] has published results of a calculation of charge disturbances around a substitutional negative impurity of unspecified nature and with tetrahedral sym-

TABLE II. Parameters of newly determined hyperfine interaction tensors of V-V^-. Data on tensors $M1$–$M13$ and $G1$-$G20$ are found in Ref. 9. Principal values A_i and reduced parameters a, b, and c are given in kHz. γ_i is the angle of the ith principal direction with the $(0\bar{1}1)$ plane; δ_i the angle between its projection on the $(0\bar{1}1)$ plane and the [100] direction. s-character fractions α^2, p-character fractions β^2, and localizations η^2 are calculated according to Eqs. (3) and (4), as discussed in Sec. II A.

Tensor	A_1	A_2	A_3	γ_1	δ_1	γ_2	δ_2	γ_3	δ_3
$M14$	525.0	365.8	351.1	0	−55.4	90		0	34.6
$M15$	434.5	316.7	234.7	0	39.3	0	−60.7	90	
$M16$	376.0	220.9	198.8	0	63.0	90		0	−27.0
$M17$	270.7	172.1	167.9	0	−57.5	0	32.5	90	
$M18$	256.0	219.4	130.5	0	20.8	90		0	−69.2
$M19$	224.3	150.4	144.5	0	54.6	0	−35.4	90	
$G21$	464.7	366.8	236.4	15.5	1.6	4.3	−89.6	73.9	−14.6
$G22$	557.5	283.8	181.5	32.4	−17.4	22.7	88.0	48.7	26.4
$G23$	479.0	299.9	181.9	27.3	−25.2	25.0	78.7	51.4	24.5
$G24$	448.1	220.3	218.4	19.2	83.7	48.7	−29.6	34.9	7.8
$G25$	395.4	336.5	152.0	2.3	22.8	1.8	−67.2	87.0	−15.7
$G26$	452.0	232.8	170.2	69.1	−60.8	11.1	60.3	17.4	−26.2
$G27$	249.5	233.2	133.0	6.2	−37.5	83.7	−26.1	1.2	52.6

Tensor	a	b	c	α^2	β^2	η^2 (%)
$M14$	413.0	55.5	7.3	0.17	0.83	0.058
$M15$	328.6	52.9	41.0	0.14	0.86	0.054
$M16$	265.2	55.4	11.1	0.12	0.88	0.055
$M17$	203.6	33.6	2.1	0.14	0.86	0.034
$M18$	202.0	−35.7	18.3	0.13	0.87	0.036
$M19$	173.1	25.6	3.0	0.15	0.85	0.027
$G21$	356.0	−59.8	49.0	0.14	0.86	0.061
$G22$	340.9	108.3	51.2	0.08	0.92	0.103
$G23$	320.3	79.4	59.0	0.10	0.90	0.077
$G24$	295.6	76.2	1.0	0.09	0.91	0.074
$G25$	294.6	−71.3	29.5	0.10	0.90	0.069
$G26$	285.0	83.5	31.3	0.09	0.91	0.080
$G27$	206.2	−36.1	8.2	0.13	0.87	0.036

TABLE III. Parameters of the M-class interactions of V-V^+ and V-V^- which belong to the chain group. Given are quotients of hyperfine parameters a/b and b/c, fractions s-character α^2 and localizations η^2 on the pertinent neighbor shells, the $\langle 111 \rangle$ crystal directions $n_\parallel$ closest to the axial direction, and the deviations δ from this direction. (The usual labeling $a = [\bar{1}11]$, $d = [\bar{1}\,\bar{1}\,\bar{1}]$ is adopted.)

Interaction	a/b	b/c	α^2	η^2 (%)	$n_\parallel$	δ (deg)
			V-V^+			
$M1$	5.3	∞	0.11	27.7	d	−0.5
$M2$	5.4	6.9	0.12	2.74	d	−0.1
$M3$	6.1	14.6	0.13	0.90	a	−8.3
$M5$	4.9	13.9	0.11	0.50	d	−4.4
$M6$	5.7	23.0	0.12	0.23	a	−6.7
			V-V^-			
$M1$	8.4	233	0.17	24.6	d	1.7
$M2$	5.8	∞	0.12	1.98	d	−1.9
$M3$	7.4	13.4	0.15	0.75	a	−4.5
$M5$	4.7	85	0.10	0.42	d	1.4
$M10$	7.3	23.0	0.15	0.21	a	−1.7
$M12$	7.2	48.5	0.15	0.100	d	3.8
$M14$	7.4	7.6	0.17	0.058	a	−0.7
$M19$	6.8	8.5	0.15	0.027	d	0.1

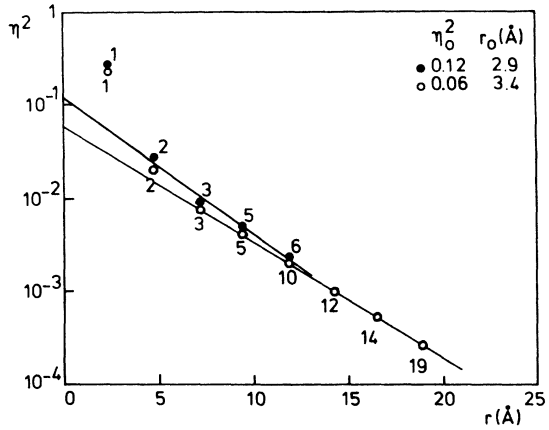

FIG. 3. Localization η^2 of the wave functions of the positive (●) and the negative (○) charge state of the divacancy. The distance is measured from the position halfway both vacancies, along the [011] zigzag chain. Numbers refer to the chosen M-type hyperfine interactions. Further details as in Fig. 1.

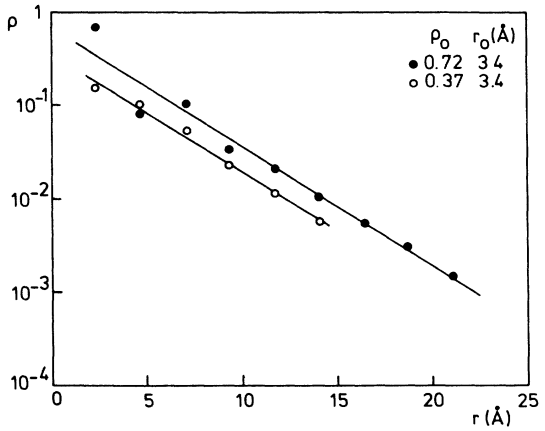

FIG. 4. Calculated charge density ρ, in fractions of an electron charge, for atom positions on ⟨011⟩ chains around an impurity in silicon, as a function of the distance to the impurity, measured along the zigzag chain. (●) Bound state shell charge for a state at $E_b=0.6$ eV above the valence band (Table III in Ref. 10). (○) Total charge for $E_b=0.4$ eV (Table IV in Ref. 10). The lines represent logarithmic fits to the formula $\rho(r)=\rho_0\exp(-r/r_0)$.

metry. First a band structure was generated in a Green's function treatment, starting with Gaussian-type atomic orbitals of s, p, and d type: $s=\exp(-\alpha r^2)$, $p_x=x\exp(-\alpha r^2)$, $d_{yz}=yz\exp(-\alpha r^2)$, etc. Next an impurity with s, p, or d character was introduced, taking a potential of diagonal form, so that the tetrahedral lattice symmetry was conserved. Subsequently, the charge density was calculated for up to 72 shells of lattice sites around the impurity. In this high symmetry, this corresponds to 1099 lattice sites. For a midgap state, the full impurity charge was found to within 1% in these shells for all types of impurity orbitals. The most striking feature of Kane's results was the strong preference with which the charge concentrates on the planar ⟨011⟩ chains of atoms, of which twelve exist in tetrahedral symmetry. In Fig. 4 we plot a small part of the results from Ref. 10 in a way similar to that in Figs. 1–3. First we take the shell charges as found for an s-type bound state at 0.6 eV above the valence band (Table III in Ref. 10). In addition, we plot the total charge (valence plus bound state) per shell for an energy level at 0.4 eV above the valence band (Table IV in Ref. 10). Especially at larger distances from the impurity site, the decrease of the charge density is exponential with a decay rate r_0 of almost exactly the same value as found for our experimental results. In the semilogarithmic plots, the calculated points by Kane can be fitted to straight lines $\rho(r)=\rho_0\exp(-r/r_0)$. The parameters of these fitted lines are included in Table IV.

TABLE IV. Parameters η_0^2 and r_0 from the fitted lines $\eta(r)^2=\eta_0^2\exp(-r/r_0)$ for the localization along the [011] chain, from Figs. 1–3. Also given are parameters for the charge density $\rho(r)=\rho_0\exp(-r/r_0)$ along ⟨011⟩ chains fitted to calculated data by Kane (Ref. 10), as shown in Fig. 4 (see figure caption). The parameter r_0 is measured along the zigzags of the chain.

Defect	η_0^2	r_0 (Å)
V^-	0.27	3.3
O-V^-	0.20	3.5
V-V^+	0.12	2.9
V-V^-	0.06	3.4
Reference 10	ρ_0	
Bound	0.72	3.4
Total	0.37	3.4

From the above observations we derive strong support for our phenomenological description of spin transfer along ⟨011⟩ zigzag lattice chains. Yet there are some differences between this theoretical approach and our experimental situation. First of all, the symmetry is different, leaving only two opposite ⟨011⟩ directions in our experiments, compared to the twelve in tetrahedral symmetry. Moreover, the local lattice structure is more strongly affected for vacancy-type defects. Nevertheless, the agreement with the vacancy-type defects is good, while a similar ⟨011⟩ preference cannot be recognized in hyperfine interactions from the tetrahedral shallow phosphorus donor in silicon, as is shown, for instance, in Fig. 2 of Ref. 1. In this case, the picture may be spoiled by the multivalley effective mass character of the electrons.

As to the physical background of the ⟨011⟩ preference, Kane refers to the importance of the so-called fifth-neighbor interaction for the description of phonon spectra in silicon. Use of central forces alone was found to give poor results for covalent solids. After the example of covalent molecules, valence force fields have therefore been introduced to describe silicon phonon spectra.[16,17] Bond lengths and bond angles between different sets of neighbor atoms are used as parameters. Solbrig[17] used

six parameters for a description of the experimentally observed silicon phonon spectra. This was not actually a real improvement with respect to the bond-charge model which was developed at about the same time and which needed only four parameters for silicon.[18] Kane, however, reassessed Solbrig's valence force approach and found that four parameters were already sufficient to produce a good fit, generally for the diamond structure.[11] In the bond-charge model, in turn, the number of required parameters depended on the substance; diamond requiring five. The most interesting finding, however, was that the third most important parameter was the fifth-neighbor interaction. A similar result was obtained when the Born–von Karman model was adopted to describe the lattice dynamics of silicon and germanium.[19] Again, addition of the fifth-neighbor interaction, as third most important parameter, was required for a satisfactory fit with experimental data. The fifth-neighbor interaction is the one which affects the two bond angles between a zigzag chain of four atoms, as illustrated in Fig. 5. Although along the chain these atoms are third neighbors, the interaction is called "fifth neighbor," because in the whole diamond lattice they constitute the fifth-neighbor distance. The ⟨011⟩ chains as discussed in this paper can be conceived as constituted by these fifth-neighbor pairs. This interaction is thus the one which resists compression and stressing of the chain. Indeed, both in theoretical studies of lattice dynamics and of thermal expansion in tetrahedrally bonded solids,[19,20] the fifth-neighbor interaction was found to be related to the shear component C_{44}, and to shear vibrations propagating along the [110] direction.

Although the kind of calculations which we refer to are not based on first principles, but are just empirical, they give a rather good insight in the physics of the processes. McMurry *et al.*,[16] for instance, make the connection between the forces which resist deformation of the lattice and the electron configuration. In a molecular orbital LCAO description, the bond angles are determined by the hybridization of the atomic orbitals. This can explain why, especially in a covalent solid, this valence force approach is so successful. In silicon a ⟨011⟩ chain constitutes an easy path for bond bending, making it understandable that the fifth-neighbor interaction is more important than the interaction between third and fourth neighbors. This will be discussed in more detail in Sec. IV.

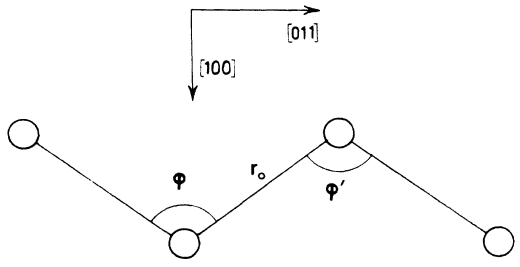

FIG. 5. Representation of the fifth-neighbor interaction $U = r_0^2 \Delta\phi \Delta\phi'$ in the silicon lattice.

IV. DISCUSSION

A. Model for vacancy-type defects

In the high symmetry of the V^- and O-V^- systems, because of the (011) mirror-plane symmetry, no experimental distinction can be made between the $\mathbf{a}=[\bar{1}11]$ and $\mathbf{d}=[\bar{1}\bar{1}\bar{1}]$ axial directions of the hyperfine interactions. This can easily be seen from Fig. 6(a), since no distinction can be made between the atom sites on both sides of the vacancy. As a result, we cannot determine for each of the sites whether the unpaired electron is accommodated in hybrid orbitals pointing backward along the chain toward the vacancy, or in orbitals pointing forward. For the divacancy the situation is different. Due to the lower symmetry we can discriminate between **a** and **d** directions. The observed directions for the chain interactions are given in Table III. Their sequence is found to be the same for V-V^+ and V-V^-. In Fig. 6(b) these directions are indicated by arrows. It follows that on the nearest neighbors the unpaired electron resides in the two dangling bonds towards the vacancies indeed, while on all next atoms it is accommodated in admixed orbitals pointing away from the center of the defect. This last observation is contrary to Lannoo's theoretical result for the one-dimensional linear semiconductor,[15] unless the so-called back-bond orbitals are admixed. This could be possible, as no experimental distinction between + or − directions can be made. In view of the further similarities between the experimental results of the various defects, we are inclined to conclude that for V^- and O-V^- the same alternation of axial directions is bound to occur. In the following we will discuss a possible relation with structural properties.

As, for instance, discussed by Phillips,[21] bond-bending forces which result from a valence-force description are related with the nature of hybridized orbitals. If there is a distortion from the tetrahedral angles, other atomic or-

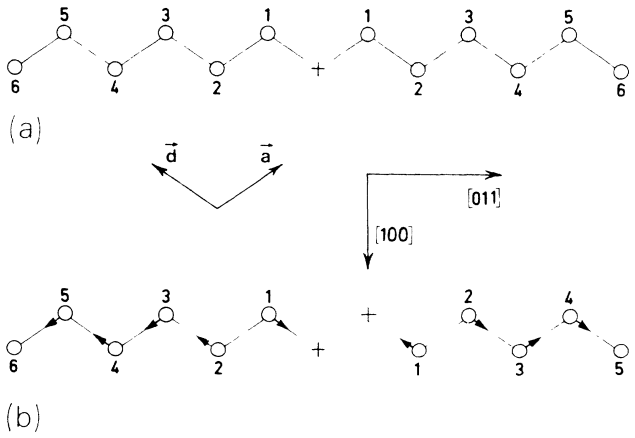

FIG. 6. Atom positions of the [011] chain in the $(0\bar{1}1)$ or *ad* plane. (a) Neighbors of the vacancy or the vacancy-oxygen complex. (b) Neighbors of the divacancy; experimentally observed axial directions of hyperfine interactions are indicated by arrows.

bitals, like $3d$, must be mixed into the original tetrahedral sp^3-hybrid valence wave functions. As the promotion energy from $3s$ and $3p$ to $3d$ is not too large, the bond-bending forces in silicon are not impassably strong, and at any rate much weaker than in diamond where $2s/2p$ to $3d$ promotion is required. If, due to some steady-state distortion, s-p-d hybridization takes place indeed, a small fraction from the originally singly occupied bonding s and p valence orbitals will become empty. Energetically, it will be rather favorable to admix these states into the wave function of the extra unpaired electron, more favorable than to admix higher-energy doubly occupied (antibonding) states.[22] In this approach a model emerges, in which the localization of the unpaired electron in the [011] chain is directly related to a structural distortion of the atoms along the chain. The relation between the electron wave function and the fifth-neighbor interaction, as manifested by structural distortions, can thus more firmly be established.

A simplified model of a distorted [011] lattice string can easily be drawn; an example is shown in Fig. 7. The first atom in the chain is shifted over a fraction δ_1 of the nearest-neighbor distance, along the $[\bar{1}11]$ direction. For the following atoms, shifts alternately along [111] and $[\bar{1}11]$ are assumed, while their mutual distances are kept constant. In this way only angles between the bonds change and nearest-neighbor bond bending is neglected, so that the distortion can be considered largely to consist of successive fifth-neighbor interactions. For small distortions, it can easily be seen that distortions for successive sites are related by $\delta_i = \frac{1}{3}\delta_{i-1}$. Consequently, the distortion decreases exponentially with distance. The decrease rate is completely determined by geometrical factors. When choosing, for instance, rather arbitrarily, alternating shifts along [233] and $[\bar{2}33]$ directions a factor $\frac{1}{2}$ results between the distortions of successive sites, just as observed experimentally for the decrease of the wave function. This picture is highly simplified, since movements of neighboring atoms next to the chain are, for instance, neglected and the relation between distortion and admixture needs not be linear either. As a result, these details bear no quantitative relevance. However, this supports the observations of exponential decrease and alternating hyperfine axis.

The only observation which requires further examination is that the hyperfine axes on the first two atom sites of the row are parallel. One should realize, however, that no distortion is required at the first-neighbor site to accommodate an appreciable fraction of the unpaired electron, since a complete dangling bond orbital at sufficiently low energy is available. This means that, as large as the distortion at the first atom may be, no direct conclusions about its direction and magnitude can be drawn from the axial direction and magnitude of the hyperfine interaction. Consequently, only the distortion direction at the second site needs to be explained and related to the hyperfine axis.

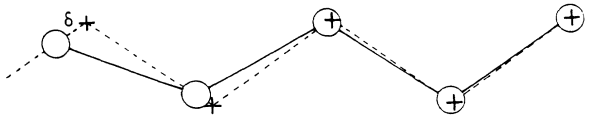

FIG. 7. Simplified representation of lattice distortions in a [011] lattice chain.

The direction of the distortion at the first neighbors, inward or outward, is not unambiguously known. From experimental data, we have tried earlier to assign one of the observed hyperfine interactions to the other two nearest-neighbor atoms b and c of the vacancy.[2,23] As nearly all spin density is symmetry forbidden at these sites, we assumed that the observed interaction arose completely from distant dipole-dipole interactions between the silicon nuclei at the forbidden sites and the high electron-spin density at the other two nearest-neighbor sites. An identification with any interaction of the right symmetry could only be made if an appreciable distortion of all four neighbors, inward to the vacancy, was assumed. Even though it was realized that the Slater orbitals that had been chosen to calculate the dipole-dipole effects were much too localized on the nuclei to properly describe dangling bond orbitals, it was concluded that an inward relaxation was required at any rate. This could not be reconciled with results from theoretical calculations for the vacancy. Four different groups all concluded independently, on the basis of different calculations that outward relaxations were bound to occur. As our assignment of the experimental hyperfine interaction involved some assumptions, we could not yet definitively prove that theoretical calculations gave the wrong result in this case. On the other hand, it seems almost impossible to construct any model in which an outward relaxation will result in a hyperfine interaction on the nearest neighbors of the order of any of the experimentally observed ones. Therefore we tend indeed to believe that an inward relaxation takes place. This relaxation will be transferred to the second and following atoms on the [011] chain.

The fact that the amount of electron localization at the first neighbor is not directly determined by the size of the lattice distortions is further reflected in the almost constant magnitude of this localization for a series of defects. Moreover, it provides an argument why this interaction needs not to fit on the curves drawn in Figs. 1–3. The fact that for V-V^- and V-V^+ these curves are at an average a factor of about 4 lower than those for V^- and O-V^-, leads to the important experimental conclusion that the distortion at the beginning of the [011] chain is appreciably smaller for divacancies than in the case of a single missing silicon atom. This strongly supports conclusions earlier drawn from consideration of Jahn-Teller energies for the vacancy.[24]

B. Other examples of fifth-neighbor electron transfer

More examples of similar fifth-neighbor interaction can be found in experimental results. First, also in G-class tensors for both V^- and O-V^-, series of interactions with the same similarities as discussed in Sec. II B, have been discerned.[2,6] In both cases the interactions have been ascribed to sites in a zigzag side chain which

branches off at position (−1,3,3), i.e., from the third site in the [011] chain. These identifications are much less firmly established, however, as alternative series can easily be conceived. A possible different identification is, for instance, one in which a series comes from the pairs of *G*-class neighbors of the consecutive [011]-chain sites. As regularities are much less conspicuous in this case, no decisive assignment in this spirit can be made, however.

Another example can be found in the ENDOR results of the boron-vacancy pair.[25] In that case conclusions could be drawn both from observed hyperfine interactions and from quadrupole interactions. The defect structure was found to consist of a vacancy with a single dangling bond at one of its neighbors and the boron atom at a next-nearest-neighbor site, lowering the defect symmetry to triclinic. From the identification of hyperfine interactions with lattice sites, it was deduced that the neutral defect has rather a B^-V^+ structure. From the eight different ^{29}Si hyperfine interactions three were found to be very similar—in the same manner as described in Sec. II B—to the largest interaction, from the dangling bond. All three had about the same magnitude, about a factor of 12 smaller than the dangling-bond interaction. Their axial directions were parallel with the dangling bond, just as at the beginning of the [011] chains. These three hyperfine interactions were therefore identified with the three neighbor atoms of the dangling-bond atom. All three of them exhibit comparable fifth-neighbor interactions with the dangling-bond atom, so that not a single [011] chain seems to exist in this lower defect symmetry. The factor of 12 difference in magnitude between the hyperfine interactions of the first and second atom in the row is comparable to the observations for both charge states of the divacancy.

From the absence of resolved hyperfine interaction, even with ENDOR, at one of the four silicon neighbors of the vacant site, it was deduced that a full electron charge was transferred from this atom to the adjoining boron, making the defect a B^-V^+ complex. From the observed boron quadrupole interaction it was derived that about 8% of the transferred electron, equally divided over both spin directions, was missing from a [111] *p* orbital at the boron, parallel to the missing dangling bond at the silicon site. The charge transfer, through a zigzag of parallel bonds at neighboring lattice sites, is probably similar to the spin transfer discussed so far. The effect may even occur as frequently, but can only be probed by nuclear quadrupole interaction which is only present at nuclei with a higher nuclear spin like boron.

C. Resulting data for the wave function outside the chain

In preceding publications[1–3] pictures of the shape of a kind of envelope of the electron wave function in all directions have been made. These were based on just the assumption of monotonic decrease with distance within each symmetry class of neighbor sites. No basic assignments of hyperfine interactions to lattice sites had been made to produce these pictures. Clearly, different envelope functions for the various symmetry classes resulted in this way. Since we have now made rather well-based identifications for lattice sites in the [011] chain of the various defects, we can plot the data for all interactions in a different way. First the chain interactions with the pertaining lattice sites are sorted out. Then the other interactions from the same mirror plane are considered, assuming again monotonic decrease with distance over the remaining sites of the class. Finally, the other symmetry types are treated in that same way. As long as no final identifications have been made for most of the other observed interactions, the assumption of monotonic decrease is the best we can do. Moreover, some deviations from monotonic decrease will have little influence on the resulting average shape of the rest of the wave function. We illustrated this earlier for phophorus in silicon, by a comparison between a plot in which the actually identified lattice positions had been used and one in which simple monotonic decrease was assumed (see Fig. 2 in Ref. 1). For a shallow, effective-masslike impurity, this assumption is much less realistic than for a deep defect, due to the occurrence of interference effects between Bloch waves from different conduction-band minima. Nevertheless, the same shape could easily be recognized in both plots.

For the chain interactions, so far, localizations η^2 had been plotted. For the other interactions this quantity is not in all cases a good measure. A number of the interactions are not axially symmetric or have parameters *a* and *b* of different signs, so that they do not comply with an LCAO analysis. Reasons for these deviations can be sought in the importance of contributions from exchange polarization or from dipolar interactions with electron densities on nearby sites.[2] In such cases just the unpaired electron density $|\Psi(r_i)|^2$ from Eq. (3), or the approximate parameter $\langle r^{-3}\rangle$ from Eq. (4), can be better taken. Therefore, both of these quantities have been plotted in the manner as discussed above. The resulting plots for all four defects (including the new data for V-V^-) are shown in Figs. 8 and 9.

The points in the plots for V^- and O-V^- clearly fall apart in three separate groups. First, of course the [011] chain interactions with a rather slow decrease rate. Secondly, the remaining interactions from the *Mad* class ("*Mad* other"), and from the general class (*G*), together form a single group. Their decrease rates with distance is much faster than in the chain. Finally, the interactions from the *Mbc* and *T* classes form together a third separate group. Their decrease rate is approximately the same, but their interactions are nearly an order of magnitude smaller than those of the previous group. This is consistent with the fact that the *Mbc* and *T* classes contain atoms in the forbidden antisymmetry plane of the wave function. From the plots for V-V^+ and V-V^- similar observations can be made. The chain interactions show the same slow decrease rate with distance as in the case of V^- and O-V^-. The remaining *M*-class interactions, together with the general class interactions, form a second group with a much faster decrease rate. A forbidden plane does not exist for these defects.

In Figs. 8 and 9 logarithmic fits to the lines $|\Psi|^2 = A_s \exp(-r/r_s)$ and $\langle r^{-3}\rangle = A_p \exp(-r/r_p)$ are drawn. Parameters of these fitted lines are given in Table

V. Except for V-V^+ the parameters for the various defects are close together. For V-V^+ however, the number of data points is rather small, so these values are not very well determined. When comparing the plots for the various defects, the "clouds" of data points which belong neither to the chain nor to a forbidden plane are seen to coincide very well for all four of them. Therefore, data points from the various defects can be combined to arrive at envelope functions which have universal validity for all of them. These values are also given in Table V.

It can be checked whether the resulting values for the "other" lattice sites are reasonable at all, by integration of their exponential envelopes over all space. The results can be divided by the free-ion wave-function parameters for silicon $3s$ or $3p$ orbitals as given in Sec. II, and by the volume which every atom takes in the silicon lattice. In this way we arrive at total electron fractions of 0.12 for s-type contributions and 0.61 for p-type contributions.

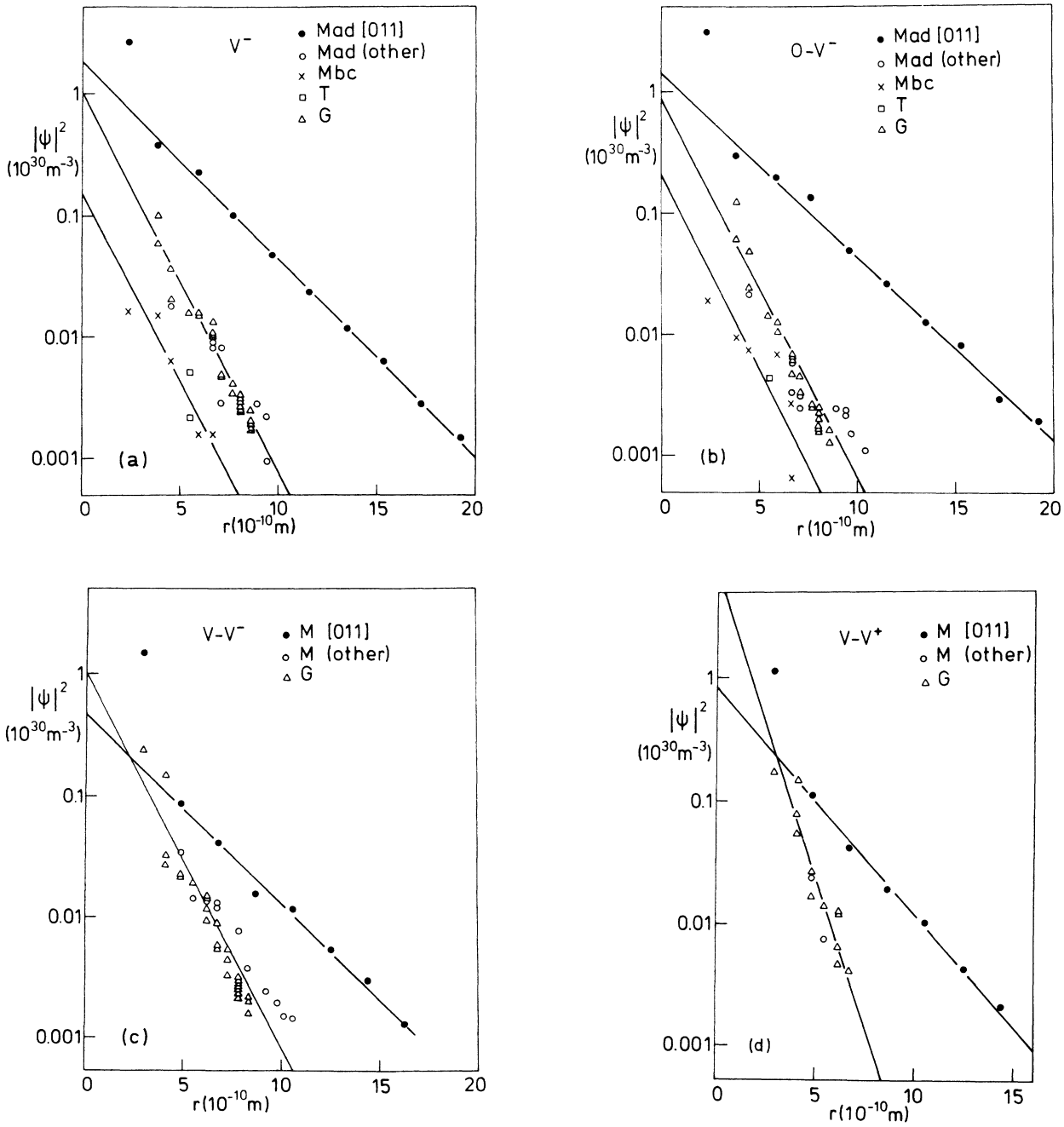

FIG. 8. Probability density $|\Psi|^2$ of the defect wave function as a function of distance to the defect center. Different classes of neighbor sites are distinguished (see text). Within each class monotonic decrease with distance is assumed. (a) Data for V^-; (b) data for O-V^-; (c) data for V-V^-; (d) data for V-V^+.

These add up to 0.73, which is only a little less than a full electron. In view of the crudeness of our approach and the uncertainties in the average parameters, the resulting universal envelopes for defect wave functions turn out remarkably trustworthy.

In this approach as well, it is interesting to compare with Kane's results.[10] Unfortunately, only few data on lattice sites outside the ⟨011⟩ chains are presented in his paper. When plotting data for s and for p orbitals for those lattice sites, from his Table III, points are even more scattered as a cloud, as can be seen in Fig. 10. Nevertheless, lines with the same decrease rates of 1.2 Å, as for our experimental points, pass reasonably well through the cloud. The same data for the chain sites, when plotted against the direct distance can be fitted very well by a straight line. Parameters for all these lines are also included in Table V. Although the s- and p-orbital type of the calculated results refers to the central impurity

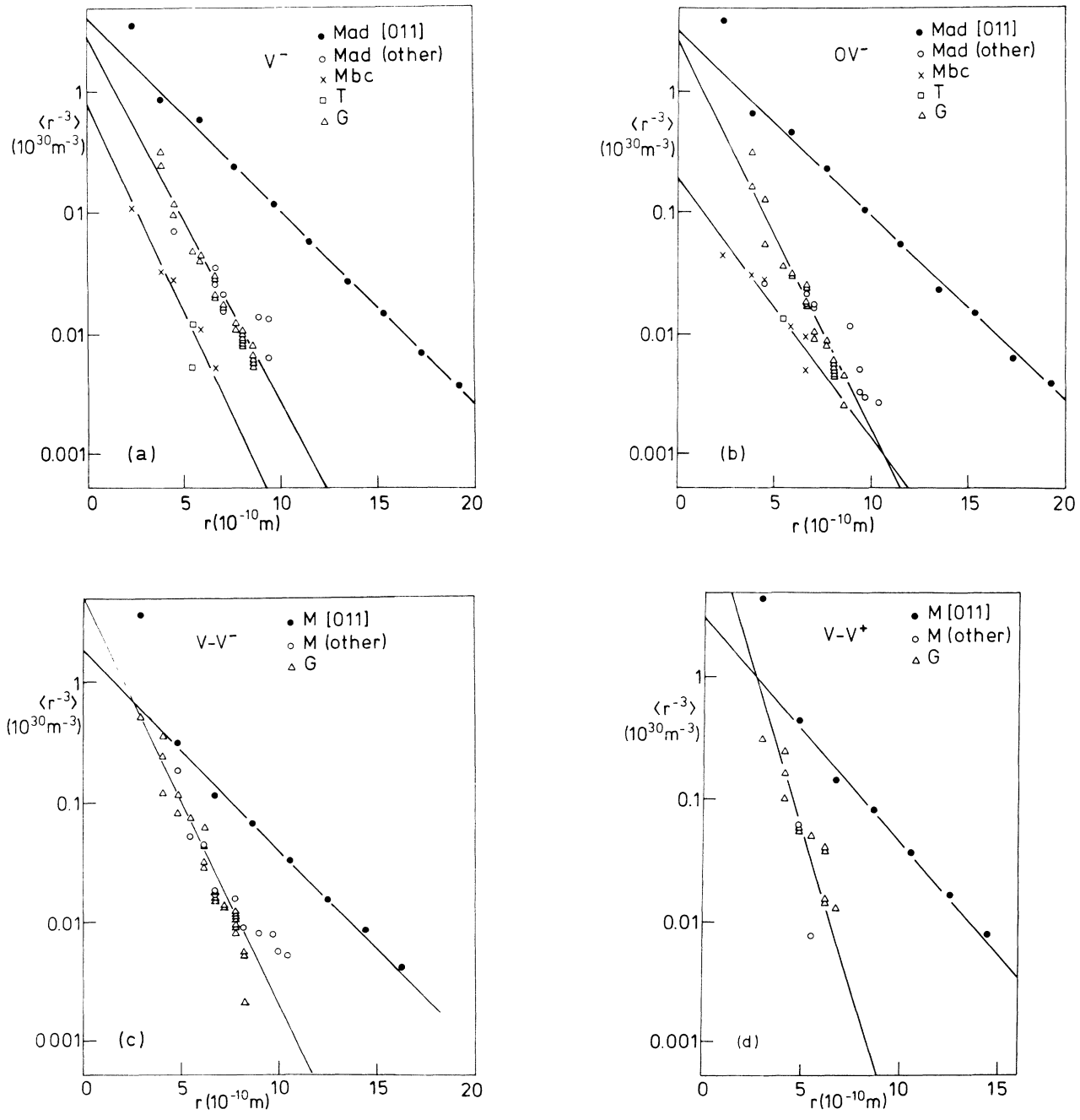

FIG. 9. Approximate value $\langle r^{-3} \rangle$, given by Eq. (4), as seen at the various lattice sites, as a function of distance to the defect center. Different classes of neighbor sites are distinguished (see text). Within each class monotonic decrease with distance is assumed. (a) Data for V^-; (b) data for O-V^-; (c) data for V-V^-; (d) data for V-V^+.

TABLE V. Parameters for fitted-wave-function shapes of vacancy-type defects in Figs. 8 and 9. Data are given separately for s and p character. Fitted curves have the forms $|\Psi|^2 = A_s \exp(-r/r_s)$ and $\langle r^{-3} \rangle = A_p \exp(-r/r_p)$. Distances are measured straight to the defect center. Distinction is made between the chain part and the rest of the wave function. The forbidden plane for V^- and O-V^- is considered separately. Data for average universal curves and for calculated charge densities by Kane (Ref. 10) in Fig. 10 are given. A_s and A_p are given in units of Å^{-3}; r_s and r_p in Å.

	[011] chain				Forbidden plane				Other			
Defect	A_s	r_s	A_p	r_p	A_s	r_s	A_p	r_p	A_s	r_s	A_p	r_p
V^-	1.8	2.7	4.2	2.7	0.15	1.4	0.8	1.3	1.0	1.4	2.9	1.4
O-V^-	1.4	2.9	3.1	2.9	0.20	1.3	0.2	2.0	0.9	1.4	2.6	1.3
V-V^+	0.8	2.3	3.1	2.4					7.9	0.9	25	0.8
V-V^-	0.5	2.8	1.8	2.6					1.0	1.4	5	1.3
Average		2.7		2.7	0.15	1.4	0.5	1.4	1.5	1.3	4	1.3
	ρ_s		ρ_p						ρ_s		ρ_p	
Reference 10	0.7	2.8	0.8	2.7					0.7	1.2	0.8	1.2

(whereas the s and p orbital type of the experimental results refers to the wave function at the neighbor shell sites), all calculational results agree very well with the experimental data.

V. CONCLUSIONS

From the present study we conclude that there exist remarkable similarities between the electronic structures of vacancy defects for which detailed hyperfine interaction data are available so far. First of all they exhibit the same one-dimensional extended spin distribution along a [011] lattice chain. At the fifth atom site of the chains, the spin density is at an average a factor of 50 larger than at sites at the same distance but in other directions. The decrease rate along the chains is nearly the same for all defects. Although regularities in the rest of the wave functions are much less pronounced, the average shape of the spin distribution in other directions is found to be similar for the various defects as well.

Theoretical data on the charge distribution around tetrahedral substitutional impurities exhibit a similarly pronounced [011] localization. Even the calculated decrease rate along the chains exactly reproduces the values found in the experimental cases. Although much less calculated data on the charge distribution at lattice sites outside the [011] chains have been presented, even these few data fit remarkably well with the average wave-function shapes derived from the experimental data.

The relation between the preference for charge and

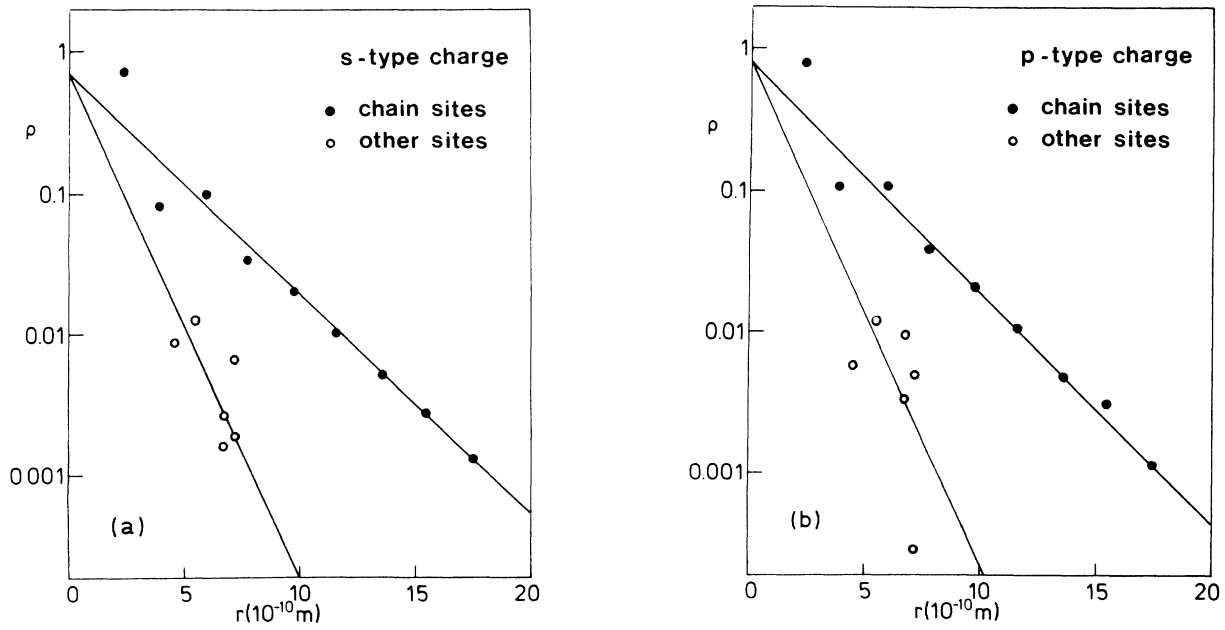

FIG. 10. Calculated charge densities ρ at atom sites around (a) an s-type and (b) a p-type impurity, as a function of the direct distance to the impurity (from Table III in Ref. 10).

spin localization along [011] chains and the so-called fifth-neighbor interaction, as already proposed by Kane, can be more substantiated by supposing a relation with structural distortions as well. The alternation of axial hyperfine directions, as derived from the observed divacancy results, can easily be explained in this manner.

An important conclusion which can be drawn from the observed extended defect structure is that special care should be taken with theoretical calculations on defect centers in silicon. Results from too small cluster calculations, or from periodic cell calculations with too small cells, will evidently be of limited importance for a complete description of the electronic structure of a defect. Moreover, structural distortions are now believed to play an important part in the eventual defect structure. Jahn-Teller effects are probably at the basis of these distortions. An indication for the relative magnitudes of these effects can then even be derived from a comparison of the absolute heights of the localization curves for [011] chains.

ACKNOWLEDGMENTS

We would like to thank H. H. P. Th. Bekman for valuable assistance with the performance and analysis of the new ENDOR measurements.

[1]E. G. Sieverts, J. Phys. C **14**, 2217 (1981).
[2]M. Sprenger, S. H. Muller, E. G. Sieverts, and C. A. J. Ammerlaan, Phys. Rev. B **35**, 1566 (1987).
[3]M. Sprenger, S. H. Muller, and C. A. J. Ammerlaan, Physica B&C **116B**, 224 (1983).
[4]G. D. Watkins and J. W. Corbett, Phys. Rev. **121**, 1001 (1961).
[5]R. van Kemp, E. G. Sieverts, and C. A. J. Ammerlaan, Mater. Sci. Forum **10-12**, 875 (1986).
[6]R. van Kemp, E. G. Sieverts, and C. A. J. Ammerlaan, Phys. Rev. B **40**, 4037 (1989); R. van Kemp, Ph.D. thesis, University of Amsterdam, 1988.
[7]J. G. de Wit, C. A. J. Ammerlaan, and E. G. Sieverts, in *Lattice Defects in Semiconductors, 1974,* edited by F. A. Huntley (The Institute of Physics, London, 1975), p. 178.
[8]J. G. de Wit, E. G. Sieverts, and C. A. J. Ammerlaan, Phys. Rev. B **14**, 3494 (1976).
[9]E. G. Sieverts, S. H. Muller, and C. A. J. Ammerlaan, Phys. Rev. B **18**, 6834 (1978).
[10]E. O. Kane, Phys. Rev. B **31**, 5199 (1985).
[11]E. O. Kane, Phys. Rev. B **31**, 7865 (1985).
[12]J. R. Morton and K. F. Preston, J. Magn. Reson. **30**, 577 (1978).
[13]M. Sprenger, Ph.D. thesis, University of Amsterdam, 1986.
[14]G. D. Watkins, in *Radiation Damage in Semiconductors,* edited by P. Baruch (Dunod, Paris, 1965), p. 97; *Radiation Damage and Defects in Semiconductors,* edited by J. E. Whitehouse (The Institute of Physics, London, 1973), p. 228.
[15]M. Lannoo and P. Lenglart, J. Phys. Chem. Solids **30**, 2409 (1969).
[16]H. L. McMurry, A. W. Solbrig, Jr., J. K. Boyter, and C. Noble, J. Phys. Chem. Solids **28**, 2359 (1967).
[17]A. W. Solbrig, Jr., J. Phys. Chem. Solids **32**, 1761 (1971).
[18]R. M. Martin, Phys. Rev. **186**, 871 (1969).
[19]J. G. Collins and N. Shiraev, in *Low Temperature Properties of Solids, Vol. 3,* edited by M. Krusius and M. Vuorio (North-Holland, Amsterdam, 1975), p. 25.
[20]A. D. Zdetsis and C. S. Wang, Phys. Rev. B **19**, 2999 (1979).
[21]J. C. Phillips, *Bonds and Bands in Semiconductors* (Academic, New York, 1973), p. 60, ff.
[22]See, for instance, R. McWeeny, *Coulson's Valence* (Oxford University Press, Oxford, 1979), p. 204, ff.
[23]E. G. Sieverts and C. A. J. Ammerlaan, Radiat. Eff. Defects Solids **111-112**, 13 (1989).
[24]G. D. Watkins, in *Lattice Defects in Semiconductors, 1974,* edited by F. A. Huntley (The Institute of Physics, London, 1975), p. 1; G. D. Watkins, J. R. Troxell, and A. P. Chatterjee, in *Defects and Radiation Effects in Semiconductors, 1978,* edited by J. H. Albany (The Institute of Physics, London, 1979), p. 16.
[25]M. Sprenger, R. van Kemp, E. G. Sieverts, and C. A. J. Ammerlaan, Phys. Rev. B **35**, 1582 (1987).